Title

Manipulating Topological Domain Boundaries in the Single-Layer Quantum Spin Hall Insulator 1T'-WSe_2.

Journal

Nano letters, 19(8)

ISSN

1530-6984

Authors

Pedramrazi, Zahra
Herbig, Charlotte
Pulkin, Artem
et al.

Publication Date

2019-08-01

DOI

10.1021/acs.nanolett.9b02157

Peer reviewed

Manipulating Topological Domain Boundaries in the Single-layer Quantum Spin Hall Insulator 1T'–WSe_2

Zahra Pedramrazi[1†], Charlotte Herbig[1†], Artem Pulkin[2,3†], Shujie Tang[4,5,6], Madeleine Philips[7,8], Dillon Wong[1], Hyejin Ryu[4,9], Michele Pizzochero[2], Yi Chen[1], Feng Wang[1,10,11], Eugene J. Mele[7], Z.X. Shen[5,6], Sung-Kwan Mo[4], Oleg V. Yazyev[2,12], M. F. Crommie[1,10,11]

[1]Department of Physics, University of California at Berkeley, Berkeley, CA 94720, USA.

[2]Institute of Physics, Ecole Polytechnique Fédérale de Lausanne (EPFL), CH-1015 Lausanne, Switzerland.

[3]Division of Chemistry and Chemical Engineering, California Institute of Technology, Pasadena, CA 91125, USA.

[4]Advanced Light Source, Lawrence Berkeley National Laboratory, Berkeley, CA 94720, USA.

[5]Stanford Institute for Materials and Energy Sciences, SLAC National Accelerator Laboratory, Menlo Park, CA 94025, USA.

[6]Geballe Laboratory for Advanced Materials, Departments of Physics and Applied Physics, Stanford University, Stanford, CA 94305, USA.

[7]Department of Physics and Astronomy, University of Pennsylvania, Philadelphia, PA 19104, USA.

[8]Center for Computational Materials Science, Naval Research Laboratory, Washington, D.C. 20375, USA.

[9]Center for Spintronics, Korea Institute of Science and Technology, Seoul 02792, Korea.

[10]Materials Sciences Division, Lawrence Berkeley National Laboratory, Berkeley, CA 94720, USA.

[11]Kavli Energy NanoScience Institute at the University of California Berkeley and the Lawrence Berkeley National Laboratory, Berkeley, CA 94720, USA.

[12]National Centre for Computational Design and Discovery of Novel Materials MARVEL, Ecole Polytechnique Fédérale de Lausanne (EPFL), CH-1015 Lausanne, Switzerland.

† These authors contributed equally to this work.

Abstract

We report the creation and manipulation of structural phase boundaries in the single-layer quantum spin Hall insulator 1T'–WSe_2 by means of scanning tunneling microscope tip pulses. We observe the formation of one-dimensional interfaces between topologically non-trivial 1T' domains having different rotational orientations, as well as induced interfaces between topologically non-trivial 1T' and topologically trivial 1H phases. Scanning tunneling spectroscopy measurements show that 1T'/1T' interface states are localized at domain

boundaries, consistent with theoretically predicted unprotected interface modes that form dispersive bands in and around the energy gap of this quantum spin Hall insulator. We observe a qualitative difference in the experimental spectral lineshape between topologically "unprotected" states at 1T'/1T' domain boundaries and protected states at 1T'/1H and 1T'/vacuum boundaries in single-layer WSe_2.

Keywords: Scanning tunneling microscopy, transition metal dichalcogenides, quantum spin hall insulators, domain boundary, ferroelasticity.

Recent experimental studies have reported the observation of the quantum spin Hall (QSH) effect in single layers of the transition metal dichalcogenides (TMDs) WTe_2 and WSe_2 in the 1T' structural phase.[1-5] Evidence of the QSH state include inverted bandgaps,[1] topologically protected edge states,[1,2,5] as well as quantized edge conduction of e^2/h per edge.[3,4] QSH edge states have been observed to reside at 1T'/1H and 1T'/vacuum boundaries, both of which are interfaces between non-trivial (1T'–TMD) and trivial (1H–TMD phase or vacuum) media.[1,2,5] Such interfaces are expected to host topologically protected edge states.[6-11] A less well-studied type of boundary in quantum spin Hall insulator (QSHI) materials is the interface between different non-trivial domains where the Z_2 topological invariant of the bulk does *not* change across the interface. We refer to a domain boundary as "topological" when there is a change in the topological invariant across the interface, and "trivial" when the invariant is the same on either side of the domain wall. A recent theoretical study of charge transport in quantum Hall insulators with trivial interfaces predicted that conduction through otherwise dissipationless quantum Hall edge states can be controllably deflected into trivial interface states, thus enabling gate-tunable charge and spin transport.[12] Single-layer TMD materials provide a new strategy for

constructing such coexisting topological and trivial interfaces by switching the layer structural phase via some local stimuli.[13-17] For example, the 1T' phase has recently been predicted to be ferroelastic in single layers, suggesting that it can be switched between different dimerization orientations by applied stress. This provides a mechanism to induce topologically trivial interfaces between QSHI domains with different crystallographic orientations. A similar strategy could allow generation of topologically non-trivial interfaces by inducing local phase switching between structures that have different Z_2 indices.[18,19]

Here we report the local phase manipulation of single-layer 1T'–WSe_2 for the purpose of creating two kinds of one-dimensional interfaces: (1) trivial interfaces between two 1T' domains and (2) topological interfaces between 1T' and 1H domains. By using scanning tunneling microscope (STM) tip pulses we are able to locally switch from the 1T' phase to the 1H phase of WSe_2, as well as between different orientations of the 1T' phase. 1T'/1T' domain-boundary formation is observed to be reversible, supporting the conjecture that single-layer 1T'–WSe_2 is a ferroelastic material.[18] Our STM measurements show that 1T'/1T' domain boundaries are well-ordered interfaces that exhibit several different structures. By combining scanning tunneling spectroscopy (STS) measurements and first-principles calculations we have determined that 1T'/1T' domain boundaries exhibit topologically unprotected one-dimensional (1D) modes that are dispersive near the Fermi level and that exhibit energy dependent decay lengths. These modes reside both inside and outside of the 1T'–bulk bandgap and, unlike 1T'/1H interface modes, do not directly connect bulk valence and conduction bands.

Mixed-phase single layers of WSe_2 were grown using molecular beam epitaxy (MBE) on bilayer graphene (BLG) supported by SiC. These samples exhibit islands that are single domains of either 1T' or 1H phase, as well as mixed-phase islands with coexisting 1T' and 1H domains.[2]

Voltage pulses applied between the STM tip and monolayer 1T'–WSe_2 islands were used to manipulate the WSe_2 structural phase. Fig. 1 shows STM topographic images of a 1T'–WSe_2 island before and after application of STM tip pulses. The "before" image (Fig. 1a) shows a single-domain region of the 1T' phase with a uniform orientation of atomic rows running from top to bottom (each row contains a zigzag chain of W atoms[1,2,9,11]). Fig. 1b shows the same region after a voltage pulse of 10 V was applied for 100 ms between the tip and surface at a constant tip-surface separation of ~6 Å. After application of the pulse the island exhibits multiple domains having different orientations that are connected by ordered 1D domain boundaries (tip pulses can also cause the formation of adsorbate clusters near domain boundaries, as shown in Fig. S7).

Because the 1T' phase can be formed in three equivalent orientations (via a Peierls distortion of its C_3-symmetric 1T parent phase) several possible 1T'/1T' domain boundaries are expected.[18] The most common 1T'/1T' interface observed in our samples is the 120° domain boundary which occurs for 85% of all observed boundaries and which connects neighboring domains rotated with respect to each other by 120° (Fig. 2a). Other observed domain boundaries are the 60° domain boundary (observed 13% of the time) and the 0° domain boundary (observed 2% of the time), as shown in Figs. 2b, c (structural models are shown in Figs. 2d-f). These well-ordered interfaces are straight-line defects that extend up to 20 nm in length in our samples. The formation of 1T'/1T' domain boundaries is reversible through the application of a high current raster scan by the STM (300mV, 1nA). Such scans remove the adsorbate clusters that form during the generation of 1T'/1T' domains, likely changing local strain distributions. This provides additional evidence of the ferroelastic nature of 1T'–WSe_2 (further details are discussed in section 6 of the SI).

The local conversion of single-layer WSe_2 from the 1T' phase to the 1H phase can be induced using the same voltage pulse method as described above. Fig. 1c shows a different single-phase 1T' island where the dimer chains run from top to bottom before applying a tip pulse, while Fig. 1d shows the same region after applying a voltage pulse of 10 V for 100 ms. The tip pulse causes an extended region of the island to convert into a new phase that exhibits reduced apparent height. We identified this region as the 1H phase of single-layer WSe_2 (see Fig. S6 for details). Such 1T' to 1H phase conversion was only observed in "confined" regions as seen here (i.e. tip-induced 1H domains were always surrounded by other material).

While 1T'/1T' domain boundaries could be created by applying tip pulses with $V_{pulse} \geq 6$ V, stronger tip pulses ($V_{pulse} \geq 10$ V) were required to locally induce the 1T' to 1H phase transition. These observations agree with predictions that the transition barrier between different orientations of the 1T' phase should be lower than the barrier for a 1T'→1H transition.[18] Tip pulses with $V_{pulse} > 6$ V often caused damage to 1T' islands, either by creating holes or by breaking apart the island. However, once 1T'/1T' and 1T'/1H domain structures are successfully induced then they remain stable under normal scan conditions.

In order to explore the electronic structure of topologically trivial interfaces in a QSHI we performed STS at the sites of the 120°, 60°, and 0° boundary structures shown in Figs. 2a-c. The dI/dV spectra obtained in the 1T' bulk (green curves in Figs. 2g-i) reflect the 1T'–WSe_2 bulk bandgap which has an average full width at half maximum (FWHM) of 85 ± 21 mV centered at –130 ± 5 mV (determination of the bulk bandgap was performed as described in Supplementary Note 3 of ref. 2). The spectral weight observed inside the bulk bandgap is explained by lifetime broadening and the –130 mV offset is due to n-doping induced by the bilayer graphene/SiC substrate, consistent with previous studies.[2,20,21] The narrow dip at V=0 seen in Figs. 2g-i likely

arises from an interplay between disorder and long-range electron-electron interactions as has been suggested previously.[2,5,20,21,27,28] This feature is more pronounced at 1D domain boundaries which is consistent with predictions regarding disorder-induced behavior in low dimensions.[28]

The spectra for the 120° and 60° domain boundaries (Figs. 2g, h) are similar in that they both have a minimum at V = 0 and exhibit broad, sloping features in the filled state regime over the range -300 mV < V_S < 0. Neither of these domain boundaries show any significant signatures of the bulk bandgap. The 0° domain boundary (Fig. 2i) also has a minimum at V = 0, but it shows a pronounced dip right in the bulk bandgap energy range. These experimental features are qualitatively different from dI/dV spectra observed at topologically-protected 1T'/vacuum and 1T'/1H boundaries where a clearly defined edge-state peak is seen at the bulk bandgap energy[2] (a reference dI/dV spectrum taken at the topological 1T'/vacuum edge is shown in Fig. S8).

Because the 120° domain boundaries are the dominant defect feature, we performed a more in-depth study of their spatially-dependent electronic structure. Fig. 3 shows dI/dV maps over the energy range -400 mV < V_s < 150 mV for a 120° 1T'/1T' domain boundary that intersects a 1T'/1H domain boundary. The first panel (Fig. 3a) shows an STM topograph of the region and includes the 120° 1T'/1T' domain boundary (dashed oval) as well as the 1T'/1H boundary (marked by a vertical dashed line with the 1T' phase to the right). This area allows us to simultaneously compare the electronic structure of "topological" and "trivial" domain boundaries.

Fig. 3b shows a dI/dV map measured at –400 mV, which corresponds to an energy below the lower edge of the bulk 1T'–WSe_2 bandgap shown in Fig. 2g (i.e., the bulk valence states). Bright intensity corresponding to high LDOS is observed at the site of the 120° domain boundary while the LDOS near the 1T'/1H interface remains low. Fig. 3c shows a dI/dV map at –120 mV,

which lies inside the 1T' bulk bandgap. At this energy high LDOS intensity is observed at both the 120° domain boundary and the 1T'/1H interface region (intensity near the 1T'/1H boundary originates from the topological edge state.[2] Fig. 3d shows a dI/dV map measured at –60 mV, which is near the upper edge of the bulk bandgap. Here high-intensity LDOS is observed near the 1T'/1H interface (from the topological edge state), while the LDOS at the 120° domain boundary shows low intensity. Fig. 3e shows a dI/dV map measured at +150 mV, which corresponds to an energy well into the bulk conduction band. At this energy neither the topological 1T'/1H interface state nor the trivial 120° domain boundary show high intensity features. The high intensity LDOS localized at the 1T'/1T' boundary in the dI/dV maps indicates the existence of defect states in the energy range $-400\ \text{mV} < V_s < -60\ \text{mV}$. The broad spectroscopic feature measured in the dI/dV point spectrum over this range for 120° domain boundaries (Fig. 2g) can thus be attributed to confined dispersive defect modes. The 120° domain boundary mode is seen to have a more strongly energy-dependent decay length than the 1T'/1H interface state and to have more intensity at lower energies.

In order to clarify the origin of these electronic features, we performed first-principles DFT simulations. The atomic structure of the interfaces was first relaxed using periodic boundary conditions in a ribbon geometry with a plane-wave basis set[22] (the relaxed structures are presented in Figs. 2d-f). We then used the non-equilibrium Green's function method (NEGF) to model the line defects with semi-infinite boundary conditions.[23,24] The resulting spin-dependent electronic band structures for the three different interfaces are presented in Figs. 4a-c. The number of bands, the dispersion, and the spin character of the defect modes changes dramatically for the different boundary types. Defect modes belonging to the 60° domain boundary (which has the least amount of symmetry) span the entire bandgap energy region while the localized

states of the 120° and 0° domain boundaries do not completely close the bulk energy gap (the bulk bandgap of the 60° domain boundary model is somewhat affected by the strain that arises from matching bulk lattice constants with the defect periodicity). We see that while the defect modes mostly close the overall energy gap for the 60° and 120° domain boundaries, the gap remains bulk-like for the 0° defect, consistent with our STM spectroscopy observations (Figs. 2g-i). The simulated 120° domain boundary states are observed to be spin-polarized out of the plane while for 60° domain boundaries the direction of spin polarization rotates for different states within the same band (colors in Figs. 4a, b). 0° domain boundaries possess inversion symmetry and so defect states associated with this boundary show no spin polarization (Fig. 4c).

Figs. 4d-f compare the calculated LDOS of the 120°, 60° and 0° domain boundaries (blue curves) with the LDOS of the 1T' bulk (grey curves) as a function of energy (the Fermi level has been shifted to match the experimentally observed n-doping). Overall we find reasonable agreement between the simulated LDOS in Fig. 4 and the corresponding STM spectroscopy measurements of Fig. 2. For example, while the experimental bulk bandgap feature vanishes for the 60° defect (Fig. 2h), an energy gap remains for the 0° defect (Fig. 2i), similar to the theory plots of Figs. 4e, f. In the 120° case the predicted small 10 meV energy gap is likely smeared out by level broadening effects that are observed experimentally but not accounted for in conventional DFT simulations.[25] When we add Gaussian broadening to our calculation then the 120° gap feature is smeared out (Fig. 4d) similar to what is seen experimentally (Fig. 2g). A significant discrepancy between the theory and the data is the pronounced LDOS peak seen near E = 0 for all three domain boundary types. By contrast, all three domain boundaries show a broad dip at V = 0 in the STM spectroscopy rather than the predicted peak. This is explained by

the coexistence of disorder and electron-electron interactions in these materials which opens a pseudogap at V = 0 eV but which is not accounted for in DFT simulations.

In conclusion, we have successfully manipulated the local electronic and structural properties of single-layer 1T'–WSe_2, thereby inducing a local phase transition from the 1T' to the 1H phase, as well as creating 1T'/1T' domain boundaries. The induced 1T'/1T'domain boundaries exhibit different rotational configurations, with a 120° domain boundary being the most common structure. Our combined STS measurements and first-principles calculations show that these new 1T'/1T' domain boundaries yield topologically unprotected 1D states that are dispersive in energy near the Fermi level and exhibit energy-dependent decay lengths. These results create new opportunities for exploring electron- and spin-based devices where charge carriers traveling along QSH edges might be deflected into trivial domain boundary modes in a controllable fashion.[12]

ACKNOWLEDGEMENT

This research was supported as part of the Center for Novel Pathways to Quantum Coherence in Materials, an Energy Frontier Research Center funded by the U.S. Department of Energy, Office of Science, Basic Energy Sciences (STM spectroscopy and dI/dV mapping). Support was also provided by the VdW Heterostructure program (KCWF16) (surface preparation and topographic characterization) funded by the Director, Office of Science, Office of Basic Energy Sciences, Materials Sciences and Engineering Division, of the US Department of Energy under Contract No. DE-AC02-05CH11231 and by the National Science Foundation under award EFMA-1542741 (local phase transition generation). The work performed at the ALS (film characterization) was supported by the Office of Basic Energy Sciences, US DOE under Contract

No. DE-AC02-05CH11231. C. H. acknowledges the support of Alexander von Humboldt Foundation for a Feodor Lynen research fellowship. The work performed at the Stanford Institute for Materials and Energy Sciences and Stanford University (MBE growth) was supported by the Division of Materials Science, Office of Basic Energy Sciences, US DOE under contract No. DE-AC02-76SF00515. Theoretical modeling of the two-channel conductance by M.P. and E.J.M. was supported by the DOE Office of Basic Energy Sciences under grant DE-FG02-ER45118. M.P. acknowledges support from an NRC Research Associateship award at the U.S. Naval Research Laboratory. S. T. acknowledges the support from the CPSF-CAS Joint Foundation for Excellent Postdoctoral Fellows. H. R. acknowledges fellowship support from NRF, Korea through Max Planck Korea/POSTECH Research Initiative No. 2016K1A4A4A01922028. A.P., M.P., and O.V.Y. acknowledge support by the ERC Starting grant "TopoMat" (Grant No. 306504) (ab initio theoretical formalism development), as well as Swiss National Science Foundation grants No. 162612 (2D bulk electronic structure) and No. 172543 (1D interface electronic structure). First-principles calculations were performed at the Swiss National Supercomputing Centre (CSCS) under project s832 and the facilities of Scientific IT and Application Support Center of EPFL. We thank Quansheng Wu for assistance with calculations, and we want to thank Canxun Zhang with helpful discussion.

REFERENCES

1 S. Tang, C. Zhang, D. Wong, Z. Pedramrazi, H. Z. Tsai, C. Jia, B. Moritz, M. Claassen, H. Ryu, S. Kahn, J. Jiang, H. Yan, M. Hashimoto, D. Lu, R. G. Moore, C. C. Hwang, C. Hwang, Z. Hussain, Y. Chen, M. M. Ugeda, Z. Liu, X. Xie, T. P. Devereaux, M. F.

Crommie, S.-K. Mo, Z. X. Shen, Quantum spin Hall state in monolayer 1T'-WTe2. Nature Physics **13**, 683, (2017).

2 M. M. Ugeda, A. Pulkin, S. Tang, H. Ryu, Q. Wu, Y. Zhang, D. Wong, Z. Pedramrazi, A. Martín-Recio, Y. Chen, F. Wang, Z. X. Shen, S.-K. Mo, O. V. Yazyev, M. F. Crommie, Observation of topologically protected states at crystalline phase boundaries in single-layer WSe2. Nature Communications **9**, 3401, (2018).

3 S. Wu, V. Fatemi, Q. D. Gibson, K. Watanabe, T. Taniguchi, R. J. Cava, P. Jarillo-Herrero, Observation of the quantum spin Hall effect up to 100 Kelvin in a monolayer crystal. Science **359**, 76, (2018).

4 Z. Fei, T. Palomaki, S. Wu, W. Zhao, X. Cai, B. Sun, P. Nguyen, J. Finney, X. Xu, D. Cobden, Edge conduction in monolayer WTe2. Nature Physics **13**, 677, (2017).

5 Z.-Y. Jia, Y.-H Song, X.-B. Li, K. Ran, P. Lu, H.-J. Zheng, X.-Y. Zhu, Z.-Q. Shi, J. Sun, J. Wen, D. Xing, S.-C. Li, Direct visualization of a two-dimensional topological insulator in the single-layer 1T'-WTe2. *Physical Review B* **96**, 041108, (2017).

6 C. L. Kane, E. J. Mele, Quantum Spin Hall Effect in Graphene. *Physical Review Letters* **95**, 226801, (2005).

7 B. A. Bernevig, S.-C. Zhang, Quantum Spin Hall Effect. *Physical Review Letters* **96**, 106802, (2006).

8 M. Z. Hasan, C. L. Kane, Colloquium: Topological insulators. *Reviews of Modern Physics* **82**, 3045, (2010).

9 X. Qian, J. Liu, L. Fu, J. Li, Quantum spin Hall effect in two-dimensional transition metal dichalcogenides. *Science* **346**, 1344, (2014).

10 Y. Ma, L. Kou, X. Li, Y. Dai, S. C. Smith, T. Heine, Quantum spin Hall effect and topological phase transition in two-dimensional square transition-metal dichalcogenides. *Physical Review B* **92**, 085427, (2015).

11 D.-H. Choe, H.-J. Sung, K. J. Chang, Understanding topological phase transition in monolayer transition metal dichalcogenides. *Physical Review B* **93**, 125109, (2016).

12 M. Phillips, E. J. Mele, Charge and spin transport on graphene grain boundaries in a quantizing magnetic field. *Physical Review B* **96**, 041403, (2017).

13 Y. Wang, J. Xiao, H. Zhu, Y. Li, Y. Alsaid, K. Y. Fong, Y. Zhou, S. Wang, W. Shi, Y. Wang, A. Zettl, E. J. Reed, X. Zhang, Structural phase transition in monolayer MoTe2 driven by electrostatic doping. Nature **550**, 487, (2017).

14 Y.-C. Lin, D. O. Dumcenco, Y.-S. Huang, K. Suenaga, Atomic mechanism of the semiconducting-to-metallic phase transition in single-layered MoS2. *Nature Nanotechnology* **9**, 391, (2014).

15 D. H. Keum, S. Cho, J. H. Kim, D.-H. Choe, H.-J. Sung, M. Kan, H. Kang, J.-Y. Hwang, S. W. Kim, H. Yang, K. J. Chang, Y. H. Lee, Bandgap opening in few-layered monoclinic MoTe2. *Nature Physics* **11**, 482, (2015).

16 R. Kappera, D. Voiry, S. E.Yalcin, B. Branch, G. Gupta, A. D. Mohite, M. Chhowalla, Phase-engineered low-resistance contacts for ultrathin MoS2 transistors. *Nature Materials* **13**, 1128, (2014).

17 Y. Li, K.-A. N. Duerloo, K.Wauson, E. J. Reed, Structural semiconductor-to-semimetal phase transition in two-dimensional materials induced by electrostatic gating. *Nature Communications* **7**, 10671, (2016).

18 W. Li, J. Li, Ferroelasticity and domain physics in two-dimensional transition metal dichalcogenide monolayers. *Nature Communications* **7**, 10843, (2016).

19 K.-A. N. Duerloo, Y. Li, E. J. Reed, Structural phase transitions in two-dimensional Mo- and W-dichalcogenide monolayers. *Nature Communications* **5**, 4214, (2014).

20 Y.-H. Song, Z.-Y. Jia, D. Zhang, X.-Y. Zhu, Z.-Q. Shi, H. Wang, L. Zhu, Q.-Q. Yuan, H. Zhang, D.-Y. Xing, S.-C. Li, Observation of Coulomb gap in the quantum spin Hall candidate single-layer 1T'-WTe2. *Nature Communications* **9**, 4071, (2018).

21 J. G. Massey, M. Lee, Direct Observation of the Coulomb Correlation Gap in a Nonmetallic Semiconductor, Si: B. *Physical Review Letters* **75**, 4266, (1995).

22 P. Giannozzi, S. Baroni, N. Bonini, M. Calandra, R. Car, C. Cavazzoni, D. Ceresoli, G. L. Chiarotti, M. Cococcioni, I. Dabo, A. Dal Corso, S. D. Gironcoli, S. Fabris, G. Fratesi, R. Gebauer, U. Gerstmann, C. Gougoussis, A. Kokalj, M. Lazzeri, L. Martin-Samos, N. Marzari, F. Mauri, R. Mazzarello, S. Paolini, A. Pasquarello, L. Paulatto, C. Sbraccia, S. Scandolo, G. Sclauzero, A. P. Seitsonen, A. Smogunov, P. Umari, R. M. Wentzcovitch, QUANTUM ESPRESSO: a modular and open-source software project for quantum simulations of materials. *Journal of Physics: Condensed Matter* **21**, 395502, (2009).

23 T. Ozaki, Variationally optimized atomic orbitals for large-scale electronic structures. *Physical Review B* **67**, 155108, (2003).

24 T. Ozaki, H. Kino, Numerical atomic basis orbitals from H to Kr. *Physical Review B* **69**, 195113, (2004).

25 V. W. Brar, S. Wickenburg, M. Panlasigui, C.-H. Park, T. O. Wehling, Y. Zhang, R. Decker, Ç. Girit, A. V. Balatsky, S. G. Louie, A. Zettl, M. F. Crommie, Observation of Carrier-Density-Dependent Many-Body Effects in Graphene via Tunneling Spectroscopy. *Physical Review Letters* **104**, 036805, (2010).

26 Y. A. Bychkov, E. I. Rashba, Properties of a 2D electron gas with a lifted spectrum degeneracy. *Phys. -JETP Lett*. **39**, 78, (1984).

27 B. L. Altshuler & A. G. Aronov, Zero bias anomaly in tunnel resistance and electron-electron interaction. *Solid State Commun.* **30,** 115, (1979).

28 L. Bartosch & P. Kopietz, Zero bias anomaly in the density of states of low-dimensional metals. *Eur. Phys. J. B* **28**, 29, (2002)

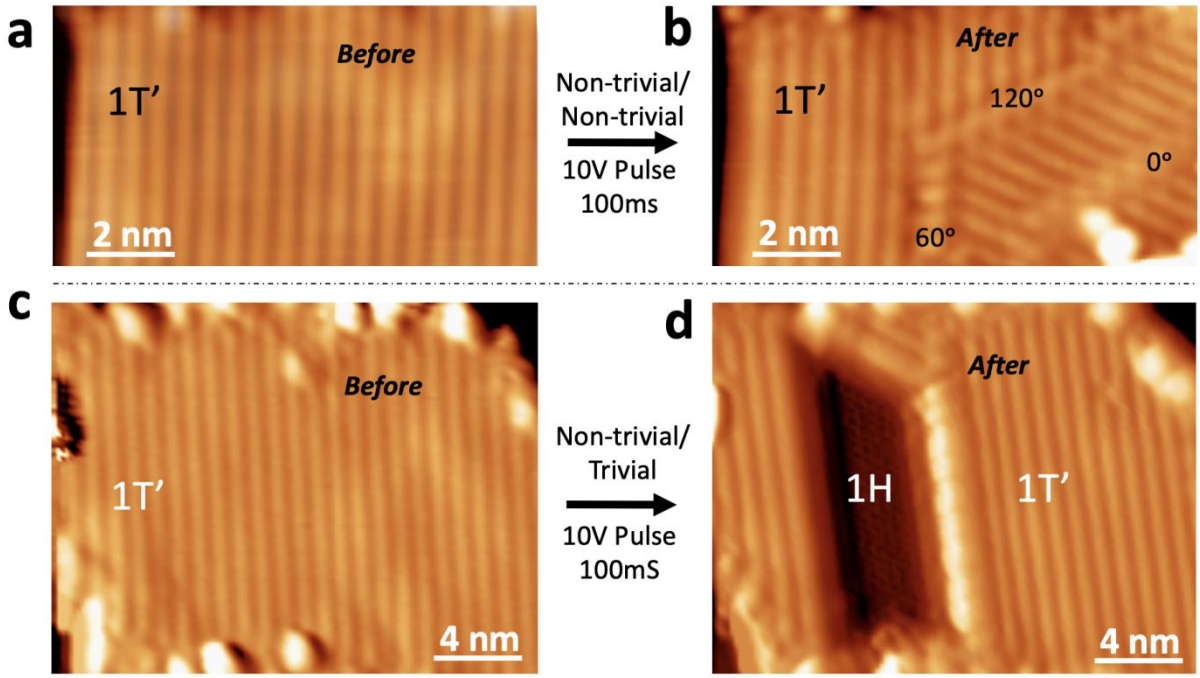

Figure 1: STM tip-induced structural change in monolayer 1T'–WSe_2. STM topographic images of a monolayer 1T'–WSe_2 island (a) before and (b) after applying a tip voltage pulse (V_{pulse}= 10 V, Δt = 100ms, tip-surface separation = 6 Å). The tip pulse creates 1T'/1T' domain boundaries having different rotational orientations. STM topographic images show a different island (c) before and (d) after an applied tip voltage pulse (V_{pulse}= 10 V, Δt = 100 ms, tip-surface separation = 6 Å) induces a 1T' to 1H structural phase transition near the center of the island. V_s = 1V , I_t =10 pA, T = 4.5 K for all images. (Image intensity here is proportional to dz/dx (where z is height) in order to enhance contrast between regions having different structural phases.)

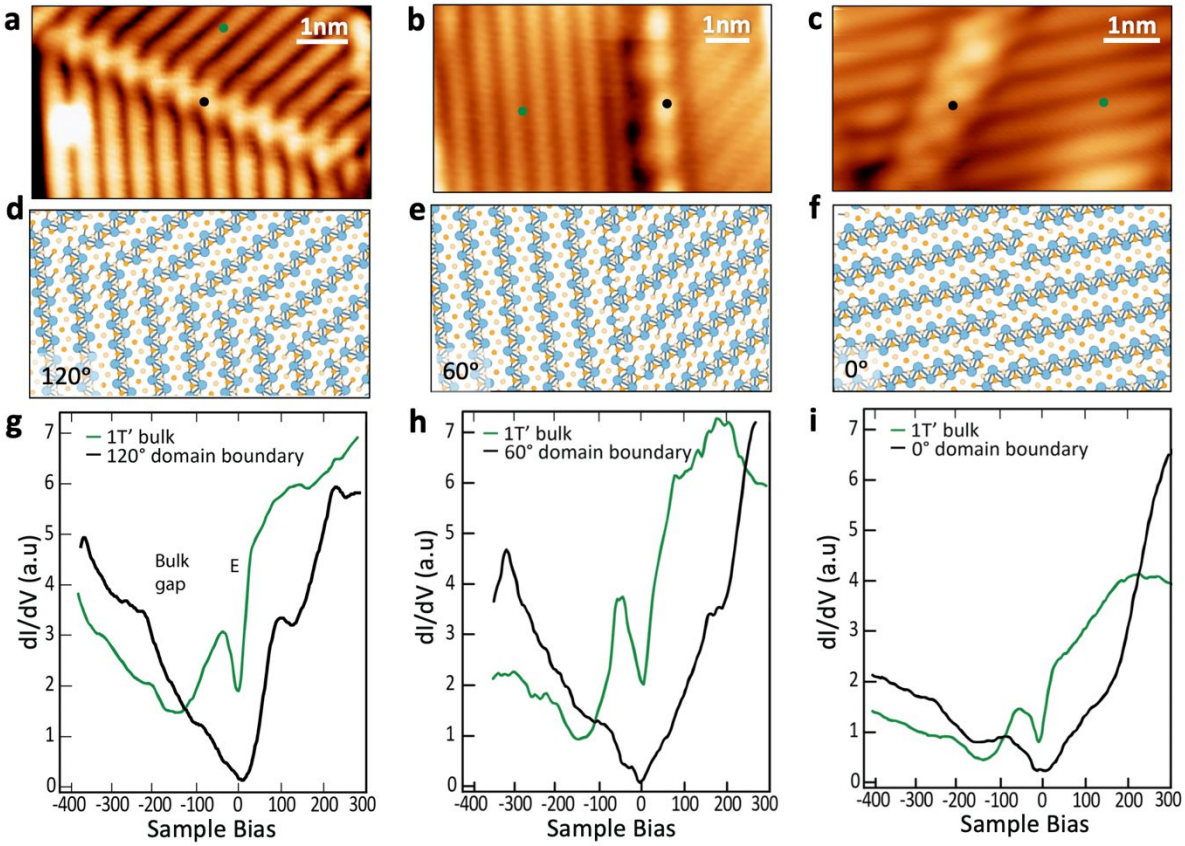

Figure 2: Structural and electronic properties of 1T'/1T' domain boundaries. STM images of (a) 120°, (b) 60°, and (c) 0° 1T'/1T' domain boundaries in 1T'–WSe_2 (V_s = 1 V, I_t = 10 pA, standard STM topographs). Relaxed structural models of (d) 120°, (e) 60°, and (f) 0° domain boundaries in 1T'–WSe_2 (calculated using DFT). STM dI/dV spectroscopy measured at (g) 120°, (h) 60°, and (i) 0° domain boundaries compared to the bulk for single-layer 1T'-WSe_2 (spectroscopy positions marked by black and green dots in (a)-(c)) (f = 613.7 Hz, V_{ac} = 4 mV, T = 4.5 K. Initial tunneling parameters for spectroscopy measurements: V_s = –400 mV, I = 100 pA).

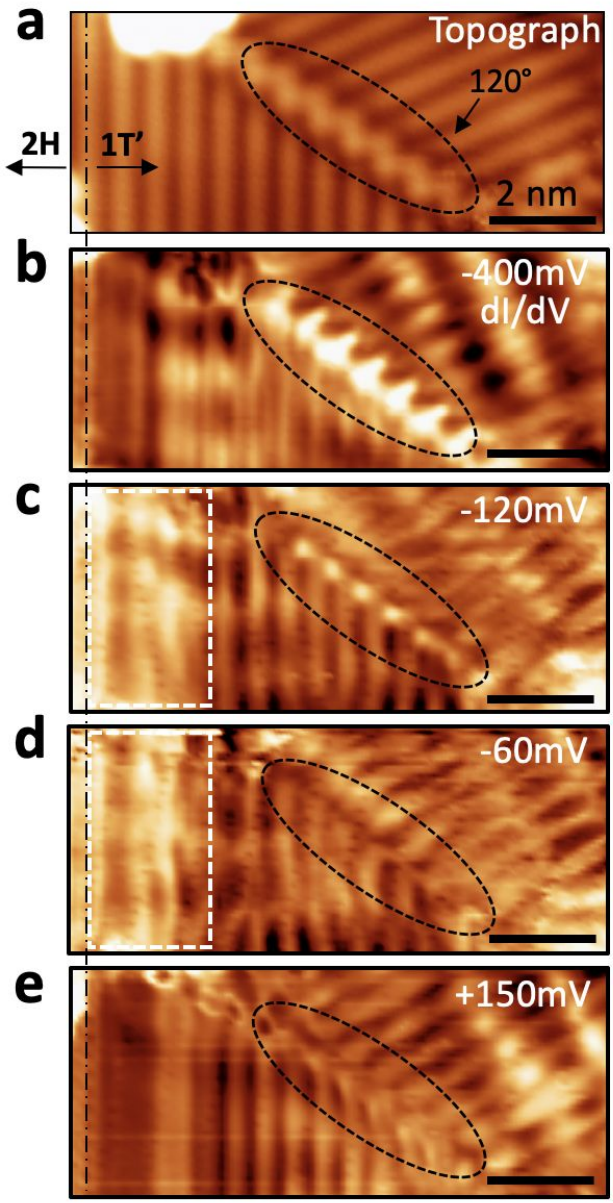

Figure 3: Comparison of electronic properties of 120° 1T'/1T' domain boundary and 1T'/1H boundary coexisting in single-layer WSe_2. (a) STM image of a mixed-phase WSe_2 island with a 120° 1T'/1T' domain boundary (standard STM topograph). The 1T'/1H interface is marked by a vertical dashed line while the 1T'/1T' interface is outlined by a dashed oval (V_s = 1 V, I_t =10 pA). dI/dV maps of the same area are shown for (b) V_s = –400 mV, (c) –120 mV, (d) –60 mV, and (e) +150 mV. Spectroscopy parameters: f = 613.7 Hz, V_{ac} = 4 mV, I = 100 pA, T = 4.5 K. Dashed white box outlines the topologically protected edge-state.

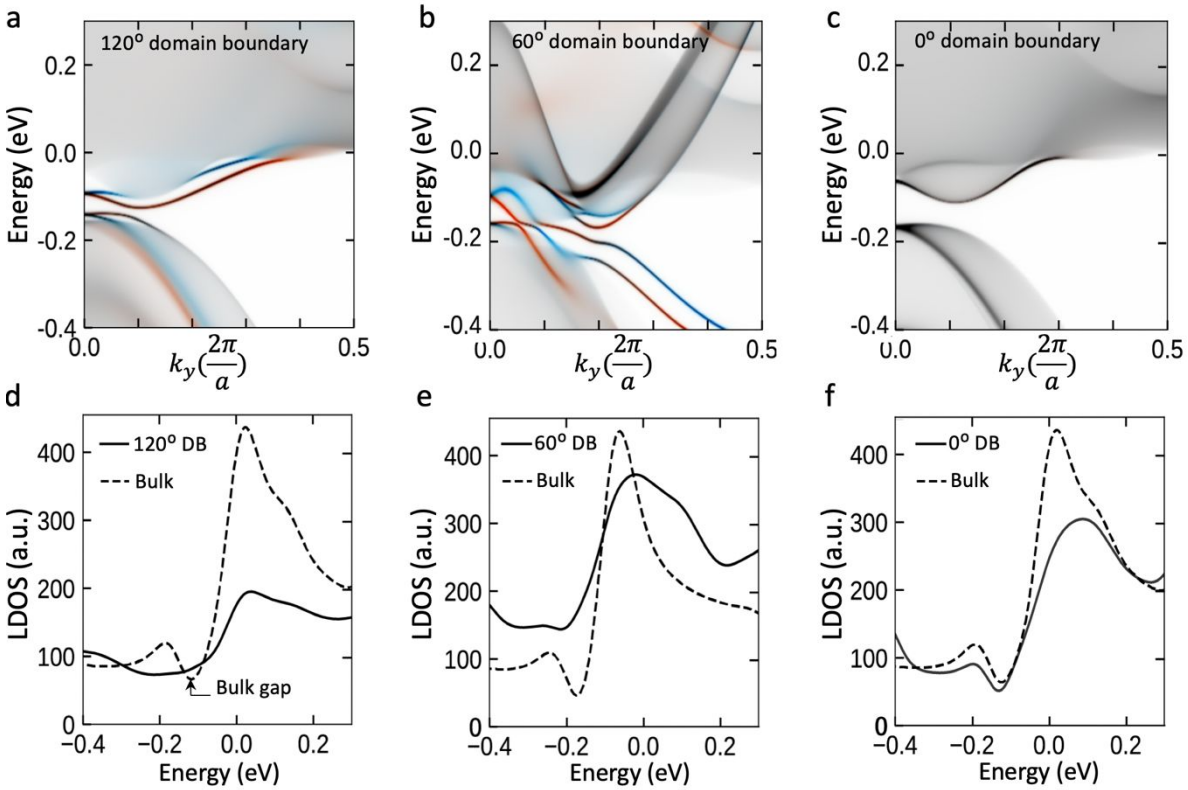

Figure 4: Calculated Band Structure and Local Density of States of Different 1T'/1T' Domain Boundaries. Calculated band structure of (a) 120°, (b) 60°, and (c) 0° 1T'/1T' domain boundaries for 1T'–WSe_2 monolayer. Bulk states are grey, spin-polarized interface modes are red and blue. (d-f) Calculated LDOS of top-layer Se atoms at a domain boundary (black solid curve) compared to LDOS in the bulk (black dashed curve) for (d) 120°, (e) 60°, and (f) 0° 1T'/1T' domain boundaries. The Fermi level (E = 0) has been shifted to match experimental data (plots presented in (d)-(f) have been convolved with a Gaussian having σ = 30 mV to simulate level broadening effects[25]).